Soil Dynamics and Earthquake Engineering, Vol. 30, No. 8, pp. 757-766, 2010

On the influence of the grain size distribution curve on P-wave velocity, constrained elastic modulus $M_{\max}$ and Poisson's ratio of quartz sands

T. Wichtmann[i], Th. Triantafyllidis[ii]

Abstract: The paper presents an experimental study on the influence of the grain size distribution curve on dynamic soil properties. More than 160 resonant column tests with additional P-wave measurements habe been performed on 27 different grain size distribution curves of a quartz sand. While the small-strain shear modulus $G_{\max}$ has been discussed by Wichtmann & Triantafyllidis [13] the present paper focusses on P-wave velocity v_P, on the small-strain constrained elastic modulus $M_{\max}$ and on Poisson's ratio ν. It is demonstrated that while v_P and $M_{\max}$ do not significantly depend on mean grain size d_{50} in the investigated range, they decrease with increasing coefficient of uniformity $C_u = d_{60}/d_{10}$ of the grain size distribution curve. Poisson's ratio does also not depend on d_{50} but increases with increasing C_u. An empirical formula similar to Hardin's equation has been developed for $M_{\max}$, considering the influence of the grain size distribution curve. It predicts quite well the experimental data.

CE Database subject headings: P-wave velocity; Constrained elastic modulus; Poisson's ratio; Quartz sand; Grain size distribution curve; Coefficient of uniformity; Resonant column tests;

1 Introduction

For feasibility studies and for final design calculations in small projects dynamic soil properties are often estimated from empirical equations (Gazetas [3]). Unfortunately, the common empirical equations for non-cohesive soils do not consider the strong influence of the grain size distribution curve (e.g. Iwasaki & Tatsuoka [9], Menq & Stokoe [11], Hardin & Kalinski [6], see a literature review given by Wichtmann & Triantafyllidis [13]).

In [13] the authors have demonstrated that the small strain shear modulus $G_{\max}$ does not depend on the mean grain size d_{50} but strongly decreases with increasing coefficient of uniformity $C_u = d_{60}/d_{10}$ of the grain size distribution curve. The well-known Hardin's equation [5, 7] (given here in its dimensionless form)

$$G_{\max} = A \frac{(a-e)^2}{1+e} {p_{\mathrm{atm}}}^{1-n} p^n \quad (1)$$

with void ratio e, mean pressure p, atmospheric pressure $p_{\mathrm{atm}} = 100$ kPa and with its commonly used constants ($A = 690$, $a = 2.17$ and $n = 0.5$ for round grains, and $A = 320$, $a = 2.97$ and $n = 0.5$ for angular grains) significantly overestimates the $G_{\max}$-values of well-graded soils. In order to extend Eq. (1) by the influence of the grain size distribution curve the following correlations of the parameters a, n and A of Eq. (1) with C_u have been developed in [13]:

$$a = 1.94 \exp(-0.066\, C_u) \quad (2)$$

$$n = 0.40\, {C_u}^{0.18} \quad (3)$$

$$A = 1563 + 3.13\, {C_u}^{2.98} \quad (4)$$

These correlations are based on more than 160 resonant column (RC) tests on 25 different grain size distribution curves with linear shape in the semi-logarithmic scale ($0.1 \le d_{50} \le 6$, $1.5 \le C_u \le 8$). In the meantime Eqs. (2) to (4) have been confirmed up to coefficients of uniformity of $C_u \approx 16$. The good approximation of the measured $G_{\max}$-data by Eq. (1) with the correlations (2) to (4) is demonstrated in [13].

Beside $G_{\max}$ a second constant (e.g. Poisson's ratio ν) is needed for an isotropic elasticity. Its dependence on the grain size distribution curve is discussed in the present paper. In order to derive correlations for the small-strain constrained elastic modulus $M_{\max} = \varrho {v_P}^2$ similar to Eqs. (2) to (4), the RC tests on the different grain size distribution curves have been supplemented by an additional measurement of the P-wave velocity v_P. Using the novel correlations for $G_{\max}$ and $M_{\max}$, Poisson's ratio ν can be estimated taking into account the grain size distribution curve.

2 Tested material

The natural quartz sand used for the present study was obtained from a sand pit near Dorsten, Germany. Its grain shape is sub-angular and the specific weight is $\varrho_s = 2.65$ g/cm^3. First, the sand was sieved into 25 gradations with grain sizes between 0.063 mm and 16 mm. Then, the grain size distribution curves shown in Fig. 1 were mixed from these gradations. They are linear in the semi-logarithmic scale. The sands and gravels L1 to L8 (Fig. 1a) had a coefficient of uniformity of $C_u = 1.5$ and different mean grain sizes d_{50} in the range $0.1 \le d_{50} \le 6$ mm. These materials were used to study the influence of d_{50}. The gravel L9 was too coarse to be tested in the RC device (specimen diameter $d = 10$ cm). The materials L24 to L26 ($d_{50} = 0.2$ mm and $2 \le C_u \le 3$), L10 to L16 ($d_{50} = 0.6$ mm and $2 \le C_u \le 8$) and L17 to L23 ($d_{50} = 2$ mm and $2 \le C_u \le 8$, Fig. 1b) were used to study the C_u-influence

[i] Research Assistant, Institute of Soil Mechanics and Rock Mechanics, University of Karlsruhe, Germany (corresponding author). Email: torsten.wichtmann@ibf.uka.de

[ii] Professor and Director of the Institute of Soil Mechanics and Rock Mechanics, University of Karlsruhe, Germany

for different values of d_{50}. The two sand-gravel-mixtures L27 and L28 (Fig. 1c) have higher coefficients of uniformity ($C_u = 12.6$ and 15.9). The d_{50}- and C_u-values as well as the minimum and maximum void ratios of the tested materials are summarized in columns 2 to 5 of Table 1.

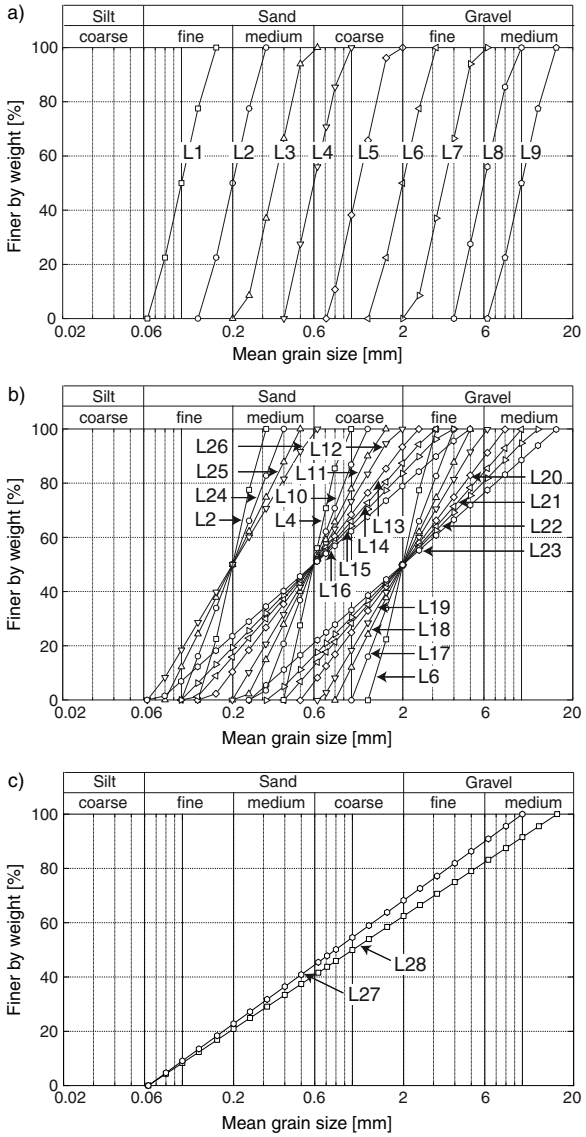

Fig. 1: Tested grain size distribution curves

3 Test device, specimen preparation and testing procedure

The resonant column (RC) device used for the present study is shown in Fig. 2. It has been explained in detail in [13]. The cylindrical specimens had a full cross section and measured $d = 10$ cm in diameter and $h = 20$ cm in height. They were prepared by air pluviation and tested under air-dry conditions.

For P-wave measurements the specimen end plates have been additionally equipped with piezoelectric elements. The transducers are similar to those explained by Brignoli et al. [1]. In all tests a single sinusoidal signal with a frequency of $f = 20$ kHz and an amplitude of 50 V was applied to the element in the base pedestal, leading to a distortion of that element in the axial direction and therefore to a P-wave traveling through the specimen in the axial direction. Both, the transmitted signal and the signal received at the transducer in the top cap, were compared at an oscilloscope (Fig. 3). The travel time t_t has been determined from the starting points of both signals (Fig. 3). Delay times in cables, amplifiers, etc. have been determined in preliminary tests and subtracted from t_t. P-wave velocity is calculated as $v_P = L/t_t$ with L being the specimen height and t_t being the corrected travel time. No wave dispersion could be found in preliminary tests on a sand similar to L4. Similar P-wave velocities were measured for frequencies of the transmitted signal between 5 kHz and 200 kHz. Therefore, the first arrival signal delivers the face velocity.

The wave lengths of the incident wave lay in the range 18 mm $\leq \lambda = v_P/f \leq$ 41 mm for all tested materials, the higher values corresponding to higher stresses and lower void ratios. The ratio λ/d_{50} of wave length and mean grain size was highest for the fine sand L1 (184 - 280) and lowest for the fine gravel L7 (6.6 - 9.4). Considering the maximum grain size, the highest ratios $\lambda/d_{\max}$ were obtained for L1 (115 - 175) and the lowest ones for L23 and L28 (1.3 to 2.6). The ratio of specimen height and wave length took values between 5.1 and 10.9 in all tests. For some materials with larger portions of coarse particles (e.g. L8, L22) the received signals were quite weak and a proper determination of v_P was impossible.

For the measurement of the small strain shear modulus $G_{\max}$ shear strain amplitudes in the range $3 \cdot 10^{-7} \leq \gamma^{\text{ampl}} \leq 10^{-6}$ were applied. Based on the literature the strain amplitudes generated in the soil using this type of P-wave sensors are also assumed to be less than 10^{-6}. In [15] we have demonstrated that the resonant column device and measurements of the S-wave velocity by means of piezoelectric elements (bender elements and shear plates) deliver similar $G_{\max}$-values.

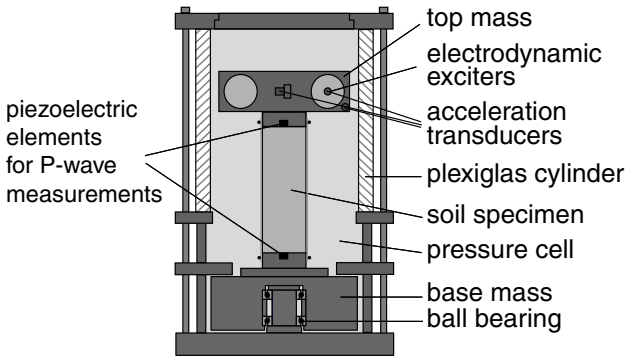

Fig. 2: Resonant Column device used for the present study, equipped with piezoelectric elements for P-wave measurements

In all tests the nearly isotropic stress was increased in seven steps (p = 50, 75, 100, 150, 200, 300 and 400 kPa). A small stress anisotropy results from the weight of the top mass ($m \approx 9$ kg). The compaction of the soil was determined by means of non-contact displacement transducers. At each pressure p the small strain shear modulus $G_{\max}$ and the P-wave velocity v_P were measured after a short resting period of 5 minutes. At $p = 400$ kPa the curves of secant shear modulus G and damping ratio D were measured as a function of shear strain amplitude γ^{ampl}. For each material several such tests with different initial relative densities

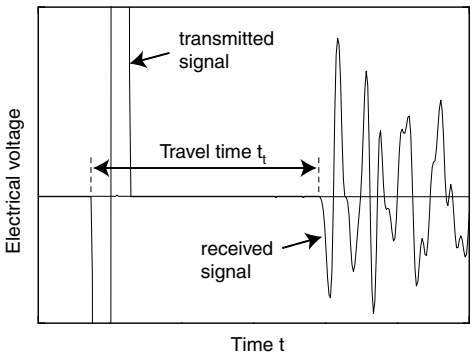

Fig. 3: Example of transmitted and received signals, interpretation of travel time t_t

$D_{r0} = (e_{\max} - e)/(e_{\max} - e_{\min})$ were performed.

4 Test results

In the following the data is discussed by means of the constrained elastic modulus $M_{\max}$. All findings apply similarly to the P-wave velocity $v_P = \sqrt{M_{\max}/\varrho}$.

Fig. 4 presents $M_{\max}$ as a function of void ratio e and mean pressure p for most of the tested materials. The diagrams show the well-known increase of the small-strain stiffness with decreasing e and with increasing p. The linear curves of $M_{\max}$ versus p in a double-logarithmic scale (Fig. 5) confirm a power-law relationship, i.e. $M_{\max} \sim p^n$.

A comparison of the $M_{\max}$-data of the uniform sands and gravels L1 to L7 (Fig. 6) reveals that for a constant void ratio and a constant pressure, $M_{\max}$ is not significantly influenced by the mean grain size. For a certain value of p, the data $M_{\max}(e)$ for different values of d_{50} fall together. In Figure 7 the small-strain constrained elastic modulus for a constant void ratio of $e = 0.70$ is plotted versus mean grain size d_{50}. Data for sand L1 are only available for larger void ratios and have thus not been included. Despite some scatter the data in Figure 7 reveals that $M_{\max}$ is almost independent of d_{50}. Only a very small tendency for $M_{\max}$ to increase with d_{50} could be concluded for larger pressures $p \geq 200$ kPa. However, it is too small to be considered in an empirical equation for $M_{\max}$.

A d_{50}-independence was observed also for the small-strain shear modulus $G_{\max}$ [13]. Analogous to $G_{\max}$, the d_{50}-independence of $M_{\max}$ can be explained micromechanically [13] on the basis of an assembly of elastic spheres using the Hertz contact theory [8].

Some studies in the literature reported higher $G_{\max}$-values for gravels than for sands (e.g. Hardin & Kalinski [6]). Based on the data from the present study an increase of $M_{\max}$ with the grain size for $d_{50} > 3.5$ mm cannot be excluded. Such coarse materials could not be tested in the available RC device. Larger specimen geometries would have been necessary. A slight increase of the small-strain stiffness with increasing d_{50} sporadically reported also for pure sands (e.g. $G_{\max}$-measurements of Menq & Stokoe [11]) is not confirmed by the results of the present study. Possibly, it could be due to variations in the grain shape.

Fig. 8 presents a comparison of the data $M_{\max}(e)$ for soils having different C_u-values. The data are shown for

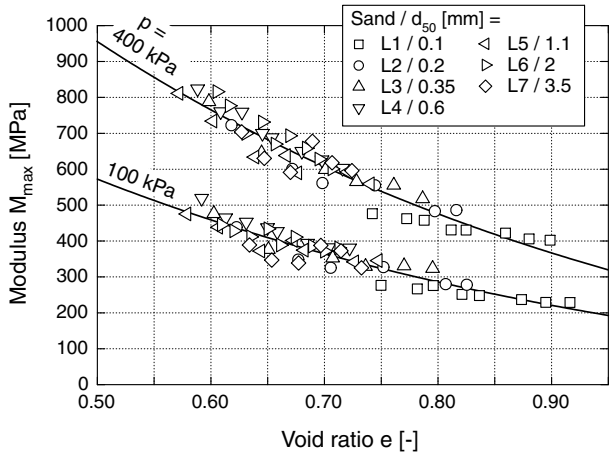

Fig. 6: Comparison of the data $M_{\max}(e)$ of sands or gravels L1 to L7 for $p = 100$ or 400 kPa, respectively

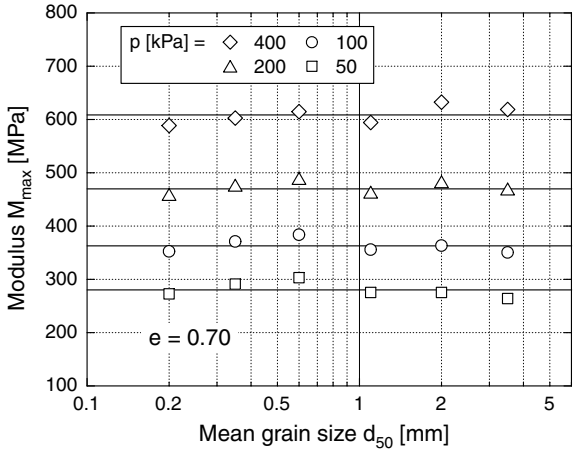

Fig. 7: Small-strain constrained elastic modulus $M_{\max}$ versus mean grain size d_{50} for a constant void ratio of $e = 0.70$

the sands with $d_{50} = 0.6$ mm, but look similar for $d_{50} = 0.2$ and 2 mm. For $e, p =$ constant, the small-strain constrained elastic modulus decreases with increasing C_u. This is also obvious in Fig. 4. It becomes even more evident from Fig. 9 where $M_{\max}$ is plotted versus C_u for $e = 0.55$. For $p = 100$ kPa the mean value is $M_{\max} = 505$ MPa for $C_u = 1.5$, while it is only $M_{\max} = 305$ MPa for $C_u = 8$ (corresponding to a 40 % decrease). For $p = 400$ kPa the values are $M_{\max} = 845$ MPa for $C_u = 1.5$ and $M_{\max} = 560$ MPa for $C_u = 8$ (34 % decrease). A somewhat larger decrease with C_u was observed for $G_{\max}$ [13].

A micromechanical explanation for the decrease of $G_{\max}$ with C_u based on the force transmission chains in mono- and polydisperse granular packings has been provided in [13]. It is also applicable to explain the observed relationship between $M_{\max}$ and C_u.

The quite large scatter of data in Figure 9 for sands having the same coefficient of uniformity C_u but different mean grain sizes $d_{50} = 0.2$, 0.6 or 2 mm, respectively, may be due to the fact that the three test series on the C_u-influence have been performed by three different persons. Slight differences in the way of pluviating the samples may have lead to deviations in the initial fabric of the samples. While the scatter is only moderate in the $G_{\max}$-measurements [13], it

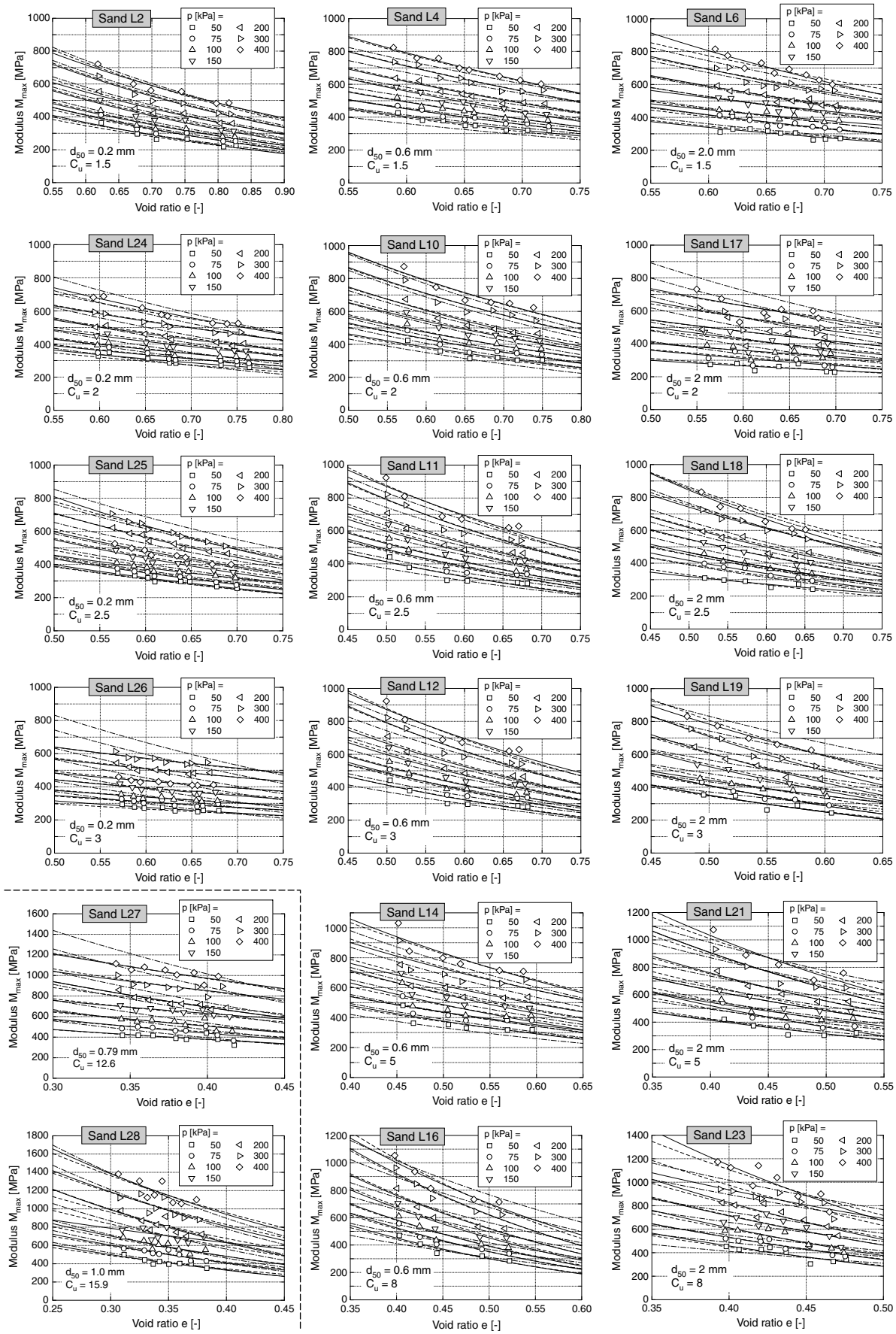

Fig. 4: *Comparison of measured and predicted constrained elastic moduli* $M_{\max}(e,p)$

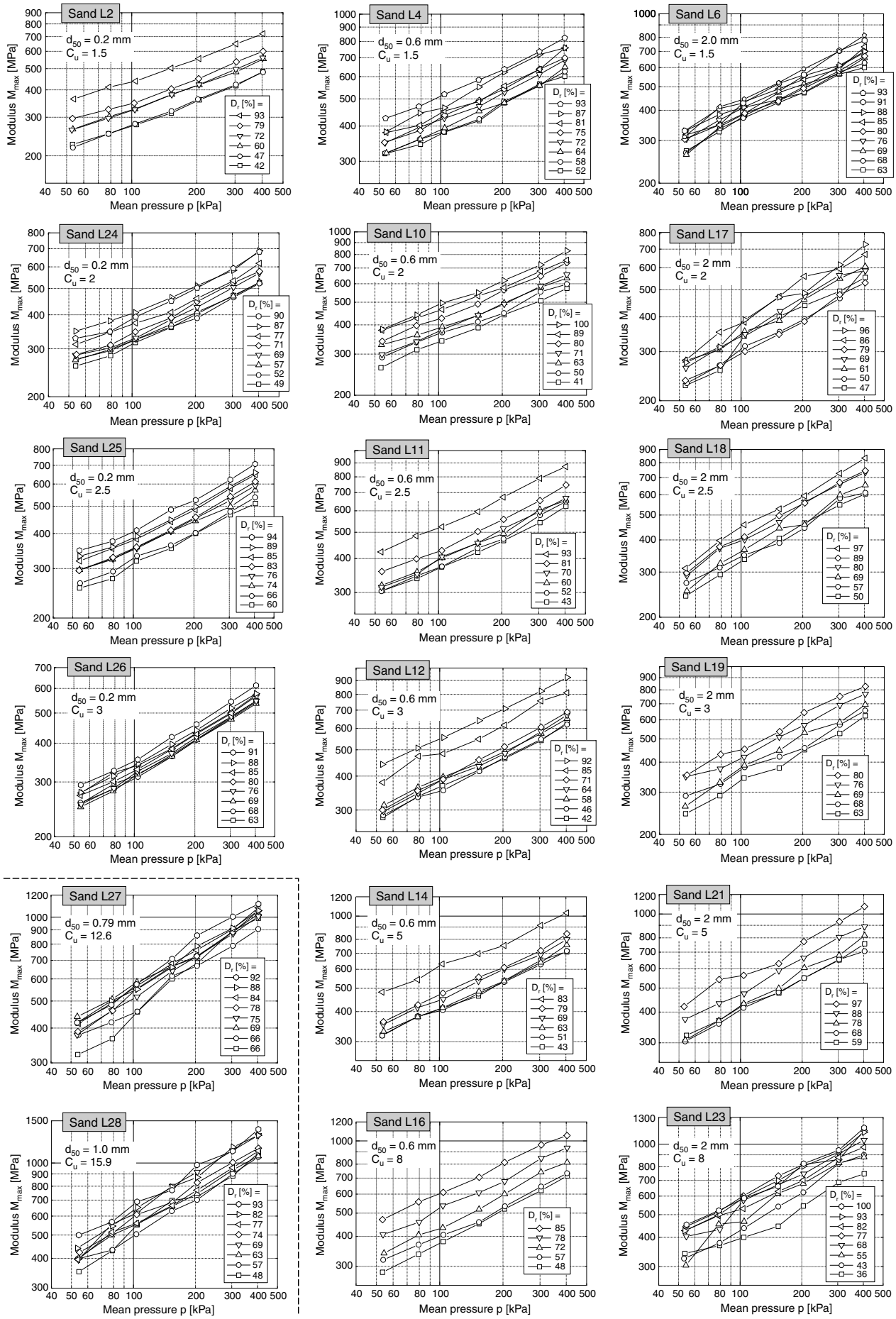

Fig. 5: *Constrained elastic modulus $M_{\max}$ as a function of mean pressure p for different initial densities D_{r0}*

is much more significant in the $M_{\max}$-data. The tests on the sands L2 to L7 were performed by the same person and therefore the samples should have the same initial fabric. Thus, the d_{50}-dependence of $M_{\max}$ may be better judged based on the data for sands L2 to L7. However, in an earlier study [14, 15] we could not find a significant influence of fabric on $G_{\max}$ or $M_{\max}$, respectively.

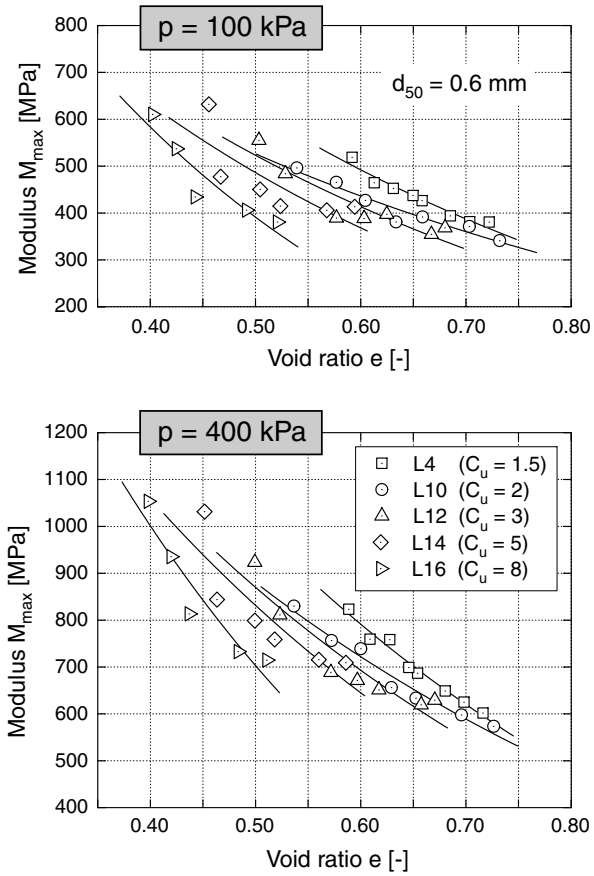

Fig. 8: Comparison of the data $M_{\max}(e)$ of sands with different C_u-values for $p = 100$ or 400 kPa, respectively

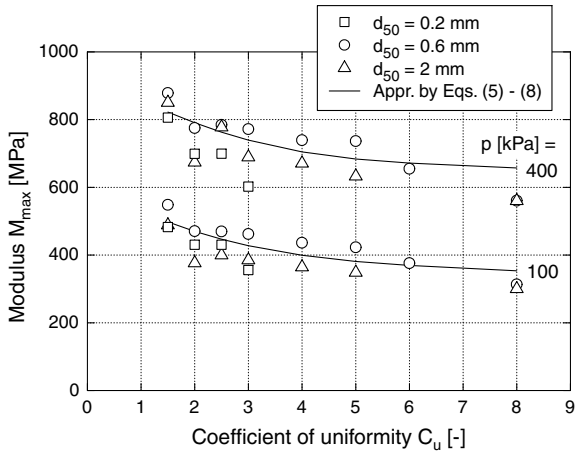

Fig. 9: Modulus $M_{\max}$ at $e = 0.55$ as a function of C_u for $p = 100$ or 400 kPa, respectively

In [13], $G_{\max}$ could be correlated with relative density D_r. This correlation is somewhat less accurate than Eq. (1) with (2) to (4). In order to derive a similar correlation for $M_{\max}$, the data has been plotted versus D_r in Fig. 10. A description of the data in the form $M_{\max}(D_r)$ seems reasonable since the minimum and maximum void ratios $e_{\min}$ and $e_{\max}$ decrease with increasing coefficient of uniformity (Table 1). However, the scatter of data in Fig. 10 is quite significant. For D_r = constant, $M_{\max}$ increases with increasing grain size. This is due to the dependence of the minimum and maximum void ratios on d_{50}, in particular due to the decrease of $e_{\max}$ with d_{50}. While the data for $d_{50} = 0.2$ mm (filled symbols in Fig. 10) lie at the lower boundary of the cloud of data, the data for $d_{50} = 2$ mm (symbols with dot) can be found at the upper boundary. For larger values of d_{50}, there is also a tendency for $M_{\max}$ to increase with C_u for D_r = constant (Fig. 10).

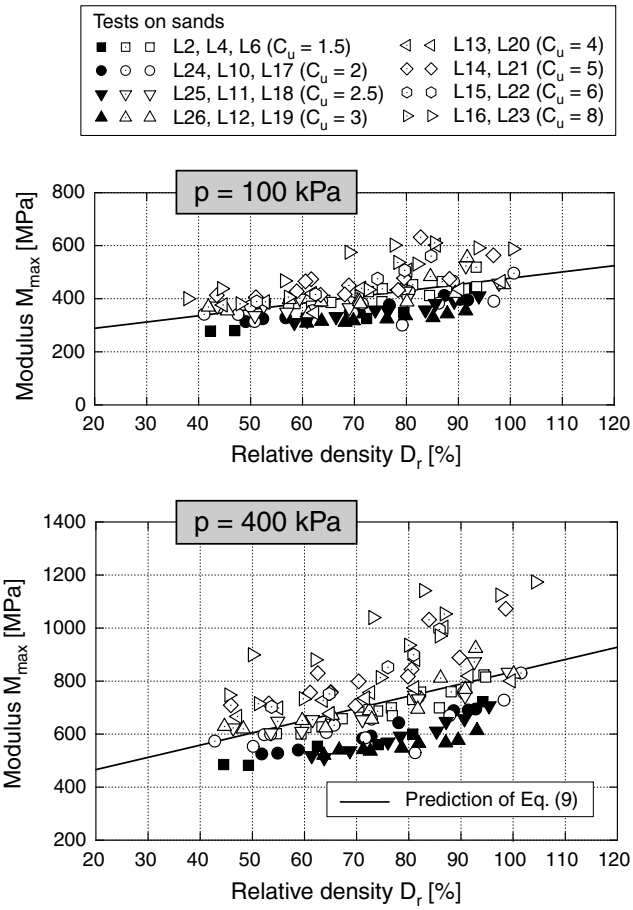

Fig. 10: Constrained elastic modulus $M_{\max}$ as a function of relative density D_r

5 Correlations for $M_{\max}$

For each tested material an equation similar to Eq. (1)

$$M_{\max} = A \underbrace{\frac{(a-e)^2}{1+e}}_{F(e)} \underbrace{{p_{\mathrm{atm}}}^{1-n}\, p^n}_{F(p)} \tag{5}$$

has been fitted to the data $M_{\max}(e, p)$. The procedure has been explained in detail in [13]. The solid curves in Fig. 4 are the best-fit curves for each pressure. The obtained parameters A, a and n have been summarized in columns 6

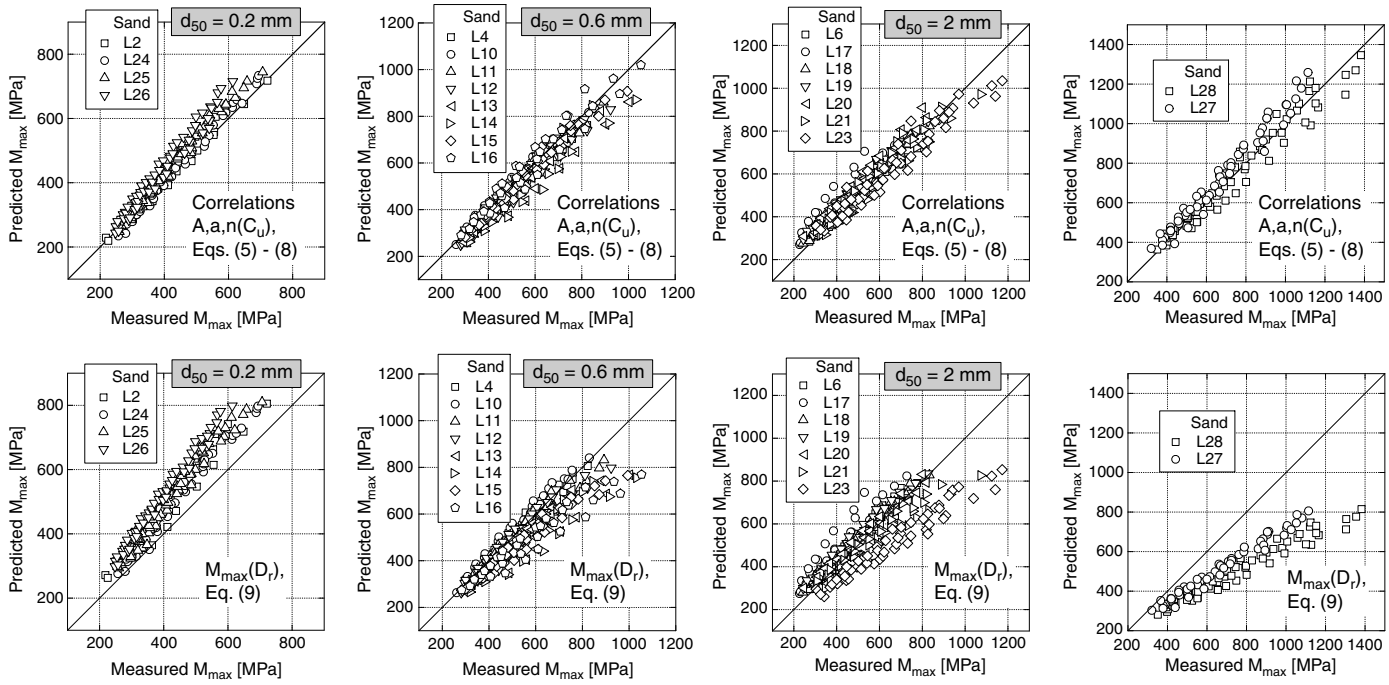

Fig. 12: $M_{\max}$-*values predicted by Eqs. (5) to (8) or by Eq. (9), respectively, versus measured moduli* $M_{\max}$ *for various sands*

to 8 of Table 1. Eq. (5) and these parameters were used to generate the dashed curves in Fig. 4. The measured and the predicted data coincide fairly well. Eq. (5) with the parameters A, a and n in columns 6 to 8 of Table 1 has also been used to generate the data points for $e = 0.55$ in Fig. 9.

In order to consider the influence of the grain size distribution curve in Eq. (5), the parameters A, a and n have been correlated with the coefficient of uniformity. Fig. 11a,b presents a and n as functions of C_u. For each material the seven values for the seven tested pressures are given. Although the scatter of data is significantly larger than in the case of $G_{\max}$ [13], a tendency for a to decrease and for n to increase with increasing C_u could be found. The data can be approximated by functions similar to Eqs. (2) and (3):

$$a = 2.16 \, \exp(-0.055 \, C_u) \quad (6)$$

$$n = 0.344 \, {C_u}^{0.126} \quad (7)$$

Re-calculating $F(e)$ and $F(p)$ in Eq. (5) with a and n obtained from Eqs. (6) and (7), the parameter A was re-evaluated and plotted versus C_u in Fig. 11c. The increase of A with increasing C_u can be described by

$$A = 3655 + 26.7 \, {C_u}^{2.42} \quad (8)$$

The parameters A, a and n calculated from Eqs. (6) to (8) have been summarized in columns 9 to 11 of Table 1.

The $M_{\max}$-values predicted by Eq. (5) with the parameters A, a and n obtained from Eqs. (6) to (8) are plotted as dot-dashed curves in Fig. 4. For most of the tested grain size distribution curves, the predicted values coincide fairly well with the measured data. An alternative presentation is given in the first row of diagrams in Fig. 12 where the predicted $M_{\max}$-values (for the same e and p) are plotted versus the measured ones. For most materials, the deviations from the bisecting line $M_{\max}^{\text{pred.}} = M_{\max}^{\text{meas.}}$ are small, confirming a good prediction of $M_{\max}$ by Eq. (5) with (6) to (8). However, the deviations between measured and predicted data are larger than in the case of $G_{\max}$ [13]. Eqs. (5) and (6) to (8) were also used to generate the solid curves $M_{\max}(C_u)$ for $e = 0.55$ in Fig. 9.

Although the scatter of data is quite significant in Fig. 10, a correlation of $M_{\max}$ with relative density D_r has also been developed:

$$M_{\max} = 2316 \left(1 + 1.07 \, \frac{D_r[\%]}{100}\right) {p_{\text{atm}}}^{1-0.39} \, p^{0.39} \quad (9)$$

As apparent from Fig. 10 (solid lines) and also from the second row of diagrams in Fig. 12 the prediction of $M_{\max}$ by Eq. (9) is less accurate than the prediction by Eq. (5) with (6) to (8). For small grain sizes $d_{50} = 0.2$ mm, $M_{\max}$ is overestimated by Eq. (9) while the stiffness for large values of d_{50} in combination with high C_u-values may be strongly underestimated, especially for sands L27 and L28 with C_u = 12.6 and 15.9, respectively (Fig. 12). Therefore, Eq. (9) should be used only for intermediate to large grain sizes ($d_{50} \geq 0.6$ mm) and small coefficients of uniformity ($C_u \leq 5$).

6 Poisson's ratio ν

Poisson's ratio ν can be calculated from

$$\nu = \frac{2 - (v_P/v_S)^2}{2 - 2\,(v_P/v_S)^2} \quad \text{or} \quad (10)$$

$$\nu = \frac{\alpha}{4(1-\alpha)} + \sqrt{\left(\frac{\alpha}{4(1-\alpha)}\right)^2 - \frac{\alpha - 2}{2(1-\alpha)}} \quad (11)$$

with $\alpha = M_{\max}/G_{\max}$. The range of ν-data for each tested grain size distribution curve is given in column 12 of Table 1. For all tested materials, ν tends to decrease with

1	2	3	4	5	6	7	8	9	10	11	12
Sand	d_{50} [mm]	C_u [-]	e_{min} [-]	e_{max} [-]	From fitting of (5) for each sand			From correlations (6) to (8)			Poisson's ratio
					A	a	n	A	a	n	ν
L1	0.1	1.5	0.634	1.127	547	3.73	0.38	3726	1.99	0.36	0.21 - 0.31
L2	0.2	1.5	0.596	0.994	3657	1.98	0.37	3726	1.99	0.36	0.24 - 0.31
L3	0.35	1.5	0.591	0.931	3172	2.11	0.35	3726	1.99	0.36	0.24 - 0.32
L4	0.6	1.5	0.571	0.891	5804	1.76	0.34	3726	1.99	0.36	0.26 - 0.33
L5	1.1	1.5	0.580	0.879	3319	2.05	0.37	3726	1.99	0.36	0.24 - 0.30
L6	2	1.5	0.591	0.877	3151	2.10	0.40	3726	1.99	0.36	0.27 - 0.32
L7	3.5	1.5	0.626	0.817	620	3.80	0.41	3726	1.99	0.36	0.25 - 0.31
L8	6	1.5	0.634	0.799	-	-	-	-	-	-	-
L10	0.6	2	0.541	0.864	2679	2.20	0.36	3798	1.94	0.38	0.26 - 0.34
L11	0.6	2.5	0.495	0.856	3280	2.04	0.37	3900	1.88	0.39	0.27 - 0.37
L12	0.6	3	0.474	0.829	5512	1.69	0.37	4036	1.83	0.40	0.28 - 0.37
L13	0.6	4	0.414	0.791	9363	1.40	0.38	4420	1.73	0.41	0.30 - 0.37
L14	0.6	5	0.394	0.749	4789	1.72	0.40	4967	1.64	0.42	0.30 - 0.39
L15	0.6	6	0.387	0.719	10366	1.30	0.40	5695	1.55	0.43	0.29 - 0.38
L16	0.6	8	0.356	0.673	17286	1.08	0.42	7748	1.39	0.45	0.28 - 0.37
L17	2	2	0.555	0.827	766	3.31	0.42	3798	1.94	0.38	0.21 - 0.30
L18	2	2.5	0.513	0.810	2829	2.03	0.48	3900	1.88	0.39	0.29 - 0.30
L19	2	3	0.491	0.783	9324	1.35	0.42	4036	1.83	0.40	0.27 - 0.32
L20	2	4	0.439	0.728	2445	2.07	0.44	4420	1.73	0.41	0.27 - 0.33
L21	2	5	0.401	0.703	9352	1.31	0.43	4967	1.64	0.42	0.29 - 0.36
L22	2	6	0.401	0.553	-	-	-	-	-	-	-
L23	2	8	0.398	0.521	22972	1.00	0.45	7748	1.39	0.45	0.31 - 0.40
L24	0.2	2	0.559	0.958	1498	2.66	0.35	3798	1.94	0.38	0.22 - 0.33
L25	0.2	2.5	0.545	0.937	3772	1.88	0.35	3900	1.88	0.39	0.25 - 0.32
L26	0.2	3	0.540	0.920	351	4.51	0.38	4036	1.83	0.40	0.20 - 0.34
L27	1.0	15.9	0.300	0.460	14668	1.07	0.51	15941	1.08	0.47	0.32 - 0.38
L28	0.79	12.6	0.327	0.564	4502	1.65	0.47	25359	0.90	0.49	0.32 - 0.39

Table 1: Parameters d_{50}, C_u, e_{min} and e_{max} (determined according to German standard code DIN 18126)) of the tested grain size distribution curves; Summary of the constants A, a and n of Eq. (5); Range of measured Poisson's ratios ν

increasing mean pressure p (Fig. 13). For small coefficients of uniformity, ν was observed to increase with increasing void ratio e while the trend emerged or even became opposite for higher C_u-values (Fig. 13).

Eq. (1) with (2) to (4) and Eq. (5) with (6) to (8) can be used to calculate Poisson's ratio ν taking into account the grain size distribution curve. ν does not depend on d_{50} since G_{max} and M_{max} do not, but it increases with increasing C_u. This becomes obvious from Fig. 14 where data for $e = 0.55$ are given (on average $\nu = 0.27$ for $C_u = 1.5$ and $\nu = 0.37$ for $C_u = 8$).

7 Summary, conclusions and outlook

The influence of the grain size distribution curve on P-wave velocity v_P, small-strain constrained elastic modulus M_{max} and Poisson's ratio ν has been studied based on more than 160 resonant column tests with an additional measurement of v_P. 27 linear grain size distribution curves of a quartz sand with mean grain sizes in the range 0.1 mm $\leq d_{50} \leq$ 6 mm and coefficients of uniformity in the range $1.5 \leq C_u = d_{60}/d_{10} \leq 15.6$ were tested. The experiments reveal that for a constant void ratio and a constant pressure, M_{max} and v_P do not significantly depend on d_{50} but strongly decrease with increasing coefficient of uniformity C_u. An empirical equation for M_{max}, similar to Hardin's equation for G_{max}, has been extended by the influence of the grain size distribution curve. For that purpose the parameters A, a and n of the formula have been correlated with C_u. It is demonstrated that the new correlations approximate quite well the measured data. A correlation of M_{max} with relative density D_r turned out to be much less accurate and can be recommended only for $d_{50} \geq 0.6$ mm and $C_u \leq 5$. Together with similar correlations developed for G_{max} [13], the novel correlations for M_{max} may be used to estimate Poisson's ratio ν, taking into account the grain size distribution curve. ν has been found independent of d_{50} but it increases with increasing C_u. For a given C_u, ν has been observed to decrease with increasing pressure.

At present we are testing bilinear, step-shaped, S-shaped or other naturally shaped grain size distribution curves of practical relevance in order to examine if the novel correlations for G_{max} and M_{max} can be applied to arbitrary grain size distribution curves. In future the correlations will also be extended by the influence of a fines content.

Acknowledgements

The presented study has been performed within the framework of the project "Influence of the coefficient of uniformity of the grain size distribution curve and of the content of fines on the dynamic properties of non-cohesive soils" funded by the German Research Council (DFG, project No. TR218/11-1). The authors are grateful to DFG for

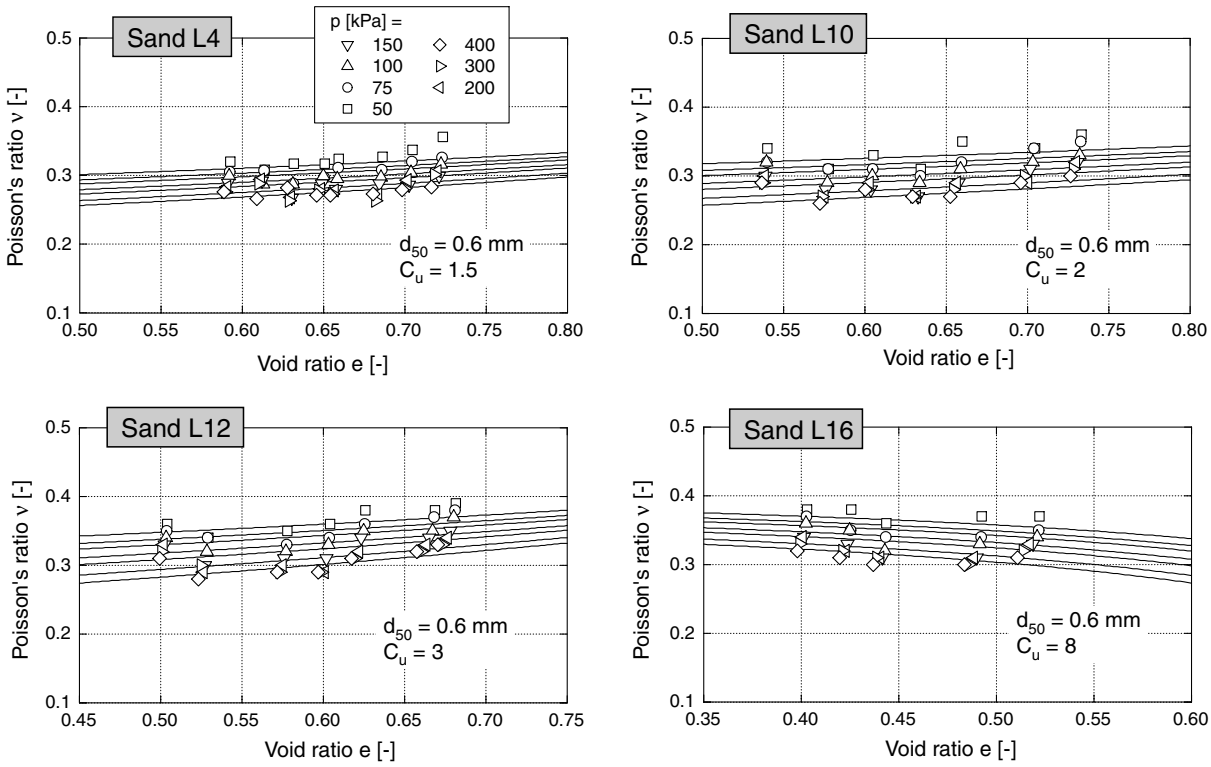

Fig. 13: *Poisson's ratio ν for four sands with different C_u-values. The solid lines were generated using Eq. (1) with (2) to (4) and Eq. (5) with (6) to (8)*

the financial support. The tests have been performed during the former work of the authors at the Institute of Soil Mechanics and Foundation Engineering at Ruhr-University Bochum, Germany. The authors gratefully acknowledge the help of the diploma thesis students R. Martinez [10], F. Durán-Graeff [2], E. Giolo [4] and M. Navarrete Hernández [12].

References

[1] G.M. Brignoli, M. Gotti, and K.H. II. Stokoe. Measurement of shear waves in laboratory specimens by means of piezoelectric transducers. *Geotechnical Testing Journal, ASTM*, 19(4):384–397, 1996.

[2] F. Duran Graeff. Influence of the coefficient of uniformity of the grain size distribution curve on the stiffness and the damping ratio of non-cohesive soils at small strains (in German). Diploma thesis, Institute of Soil Mechanics and Foundation Engineering, Ruhr-University Bochum, 2008.

[3] G. Gazetas. *Foundation Engineering Handbook, 2nd Edition*, chapter 15: Foundation vibrations, pages 553–593. 1991.

[4] E. Giolo. Influence of the coefficient of uniformity of the grain size distribution curve on the stiffness and the damping ratio of non-cohesive soils at small strains (in German). Project thesis, Institute of Soil Mechanics and Foundation Engineering, Ruhr-University Bochum, 2008.

[5] B.O. Hardin and W.L. Black. Sand stiffness under various triaxial stresses. *Journal of the Soil Mechanics and Foundations Division, ASCE*, 92(SM2):27–42, 1966.

[6] B.O. Hardin and M.E. Kalinski. Estimating the shear modulus of gravelly soils. *Journal of Geotechnical and Geoenvironmental Engineering, ASCE*, 131(7):867–875, 2005.

[7] B.O. Hardin and F.E. Richart Jr. Elastic wave velocities in granular soils. *Journal of the Soil Mechanics and Foundations Division, ASCE*, 89(SM1):33–65, 1963.

[8] H. Hertz. Über die Berührung fester elastischer Körper. *Journal reine und angewandte Mathematik*, 92:156–171, 1881.

[9] T. Iwasaki and F. Tatsuoka. Effects of grain size and grading on dynamic shear moduli of sands. *Soils and Foundations*, 17(3):19–35, 1977.

[10] R. Martinez. Influence of the grain size distribution curve on the stiffness and the damping ratio of non-cohesive soils at small strains (in German). Diploma thesis, Institute of Soil Mechanics and Foundation Engineering, Ruhr-University Bochum, 2007.

[11] F.-Y. Menq and K.H. Stokoe II. Linear dynamic properties of sandy and gravelly soils from large-scale resonant tests. In Di Benedetto et al., editor, *Deformation Characteristics of Geomaterials*, pages 63–71. Swets & Zeitlinger, Lisse, 2003.

[12] M. Navarrete Hernandez. Influence of the content of fines of a non-cohesive soil on the stiffness and the damping ratio at small strain amplitudes (in German). Diploma thesis, Institute of Soil Mechanics and Foundation Engineering, Ruhr-University Bochum, 2009.

[13] T. Wichtmann and T. Triantafyllidis. On the influence of the grain size distribution curve of quartz sand on the small strain shear modulus $G_{\max}$. *Journal of Geotechnical and Geoenvironmental Engineering, ASCE*, 135(10):1404–1418, 2009.

[14] T. Wichtmann and Th. Triantafyllidis. Influence of a cyclic and dynamic loading history on dynamic properties of dry sand, part I: cyclic and dynamic torsional prestraining. *Soil Dynamics and Earthquake Engineering*, 24(2):127–147, 2004.

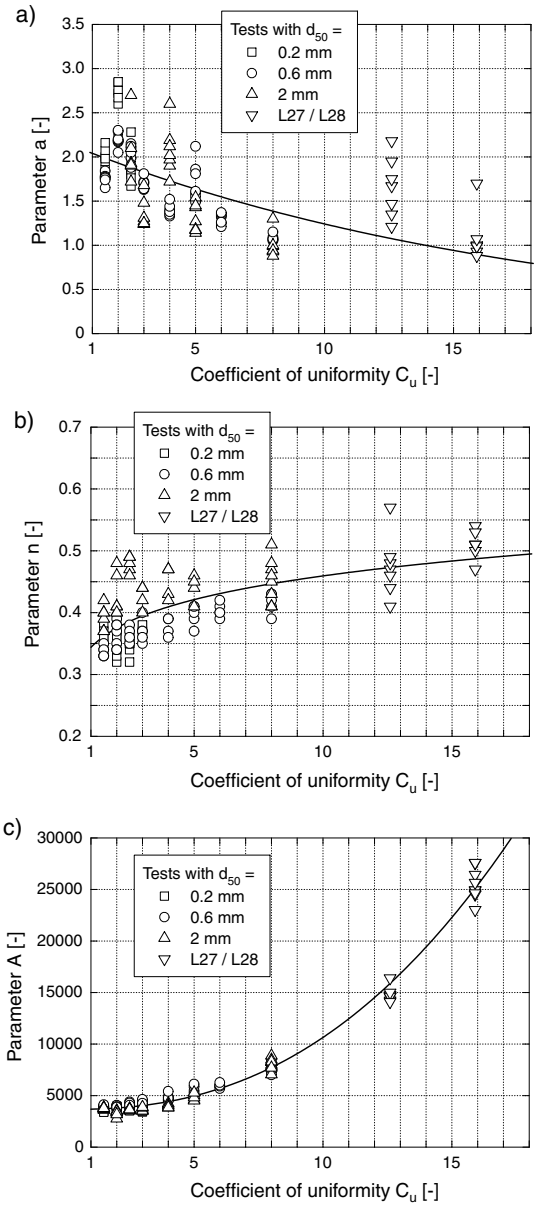

Fig. 11: Correlations of the parameters a, n and A in Eq. (5) with the coefficient of uniformity C_u

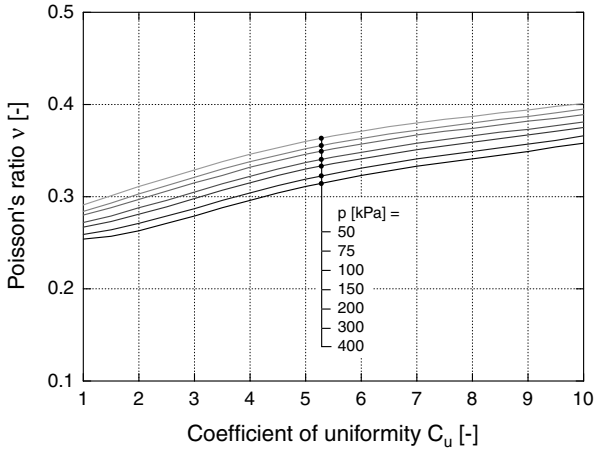

Fig. 14: Poisson's ratio ν for a constant void ratio $e = 0.55$ as a function of the coefficient of uniformity C_u, ν-values calculated with Eqs. (1) to (4) and (5) to (8)

[15] T. Wichtmann and Th. Triantafyllidis. Influence of a cyclic and dynamic loading history on dynamic properties of dry sand, part II: cyclic axial preloading. *Soil Dynamics and Earthquake Engineering*, 24(11):789–803, 2004.